Published in IET Microwaves, Antennas & Propagation
Received on 19th February 2013
Revised on 16th June 2013
Accepted on 18th June 2013
doi: 10.1049/iet-map.2013.0102

ISSN 1751-8725

Effect of antenna array properties on multiple-input–multiple-output system performance in an underground mine

Arghavan Emami Forooshani, Robert D. White, David G. Michelson

Electrical and Computer Engineering, University of British Columbia, Vancouver, Canada
E-mail: arghavan@ece.ubc.ca

Abstract: There is no deployment strategy or capacity prediction available for wireless multiple-input–multiple-output (MIMO) communication systems inside underground mines. In such environments with low angular spread, the authors showed how antenna properties including antenna spacing, polarisation and height impact a 4×4-MIMO system performance. They used channel-frequency-response data near the 2.4 GHz obtained from measurements collected in a short underground mine, along with the recently developed multimode waveguide model. Several uniform-linear-array configurations were assessed for various propagation scenarios in the mine. They used the singular value, correlation coefficient and capacity analysis to compare their performance. Based on the results, they proposed an array orientation and element spacing, which provides sufficient spatial decorrelation among MIMO subchannels. The spatial decorrelation results are close to that of an i.i.d. Rayleigh channel and are not sensitive to different propagation scenarios. The authors' study of the array height and element polarisation revealed that they mainly impact the subchannels' power, which leads to offering different MIMO channel capacities. They also observed that in spite of geometrical dissimilarities between underground mines and large tunnels, some of their measurement results in the mine are similar to those of subway tunnels obtained by previous studies.

1 Introduction

Multiple-input–multiple-output (MIMO) systems are a well-proven wireless technology for use in surface environments, where they offer higher data rates, greater coverage and increased reliability for line-of-sight (LOS) and non-LOS (NLOS) scenarios compared with older technology. Nevertheless, their performance is uncertain in confined spaces, such as underground mines. The rapid growth of MIMO-based technologies (e.g. reconfigurable antennas, advanced space-time coding schemes, multi-user MIMO) in the past decade has made it more crucial to resolve physical layer limitations when deploying MIMO systems into new environments to maximise performance.

Currently, most underground mines are equipped with legacy communication systems, such as leaky feeders that suffer from limited coverage, low data rates and require an LOS path. These limitations make MIMO technology an attractive solution for wireless communications inside mines because MIMO has overcome these problems in surface environments. However, MIMO-based systems are highly dependent on the surrounding physical environment. Therefore conventional MIMO-based wireless devices that work well in surface environments do not necessarily work well in underground mine tunnels, where propagating signals are characterised by a low angular spread.

Unlike the extensive MIMO studies conducted for indoor and outdoor environments, only a few experimental studies have been conducted for underground environment, such as subway tunnels [1–4] and underground mines [5]. In [5], as the only experimental MIMO study in underground mines, performance of a 2×2-MIMO system for two types of antenna radiation patterns has been compared in a very short underground mine (25 m). However, further investigation of antenna properties and the effect of the mine structure (e.g. curvature) on the channel capacity are required. Relevant studies for subway tunnels have focused on access-point (AP)-to-mobile communications at 900 MHz [1], in which transmitter antennas are on the platform and receiver antennas are located on the train windshield. Although previous studies confirm that MIMO can be a promising technology for AP-to-mobile applications in underground environments, too many uncertainties still remain. For example, there is no performance prediction, array design, deployment strategy or channel prediction available for MIMO-based AP communications inside underground mines. In addition, because of geometric dissimilarities between mines and subway tunnels, the applicability of results obtained from tunnels to mines, is questionable.

In response to these uncertainties, we have conducted both theoretical and experimental MIMO performance analysis for underground mines. We have evaluated MIMO-based AP communications and answered some of the questions left in the literature. We have also shown how antenna properties (e.g. antenna spacing, polarisation and height) impact

wireless performance, and thus should be carefully considered in array configuration designs and deployments inside mines.

We have experimentally evaluated the MIMO system performance in an actual mine site, and study the impact of other antenna properties, such as height and polarisation. By employing different normalisation methods on the channel coefficient matrix (***H***-matrix), we have differentiated the ways that antenna properties impact the capacity (the spatial structure or the power). We have also studied the effect of mine curvature on the MIMO channel capacity.

We have compared the experimental results in the mine tunnel with a theoretical model based on the waveguide theory (multimode waveguide model) [6], which was developed to underground tunnels and claims to be applicable to underground mine tunnels. Our experimental work matches well with this model, and confirms its applicability to underground mine tunnels. We have used this model to achieve physical insights and explain our experimental results. Additionally, this model allows us to evaluate the channel capacity of several antenna spacings and accordingly determine the proper antenna spacing for MIMO-based systems.

Finally, we conclude the paper by providing results that can be useful in developing guidelines for MIMO system deployments in underground mines. The remainder of this paper is organised as follows. In Section 2, we describe the measurement site, our setup and measurement scenarios. In Section 3, the multiple antenna analysis used in this study is presented. In Section 4, results and impact of antenna properties, which can be used in MIMO system deployment in underground mines are discussed. Finally, in Section 5, we conclude the paper by presenting key findings and their implications.

2 MIMO measurement in an underground mine

2.1 Measurement site and equipment

We performed a MIMO measurement campaign at Myra Falls underground mine located in Strathcona Park on Vancouver Island, B.C., Canada (Fig. 1). The mine gallery was 1900 ft (579 m) below the surface. The cross-sectional shape of the tunnel was rectangular. The width and height of the tunnels varied from 5 to 5.7 m and from 3.5 to 4.2 m, respectively. The mine's floor was covered in mud, and the only infrastructure were leaky feeder cables, wires and pipes installed along the ceiling. The sidewalls were not perfectly straight, had several protrusions but their roughness was insignificant. We had the opportunity to conduct static measurements because the mine-level was closed and nobody was working there.

For this study, we used our MIMO ultra-wide-band (UWB) channel sounder system. It uses the virtual array method, in which mutual coupling effect of the antenna elements is not included in the channel characterisation. Although this channel sounder performs UWB measurements, the results and analysis presented in this work focuses on MIMO characterisation at frequencies near the 2.4 GHz, industrial–scientific–medical band. We used a bandwidth of about 100 MHz in order to focus solely on the study of MIMO array properties at a chosen frequency (2.49 GHz) without concerning ourselves with the changes of the antenna element spacing with respect to the wavelength (2λ).

We used an Anritsu MS2034A vector-network-analyser (VNA) to send and receive frequency span of 2.49–4 GHz with 551 frequency points. Two UWB biconical antennas were used, one at the transmitter and one at the receiver. The transmitter antenna was manually moved across the

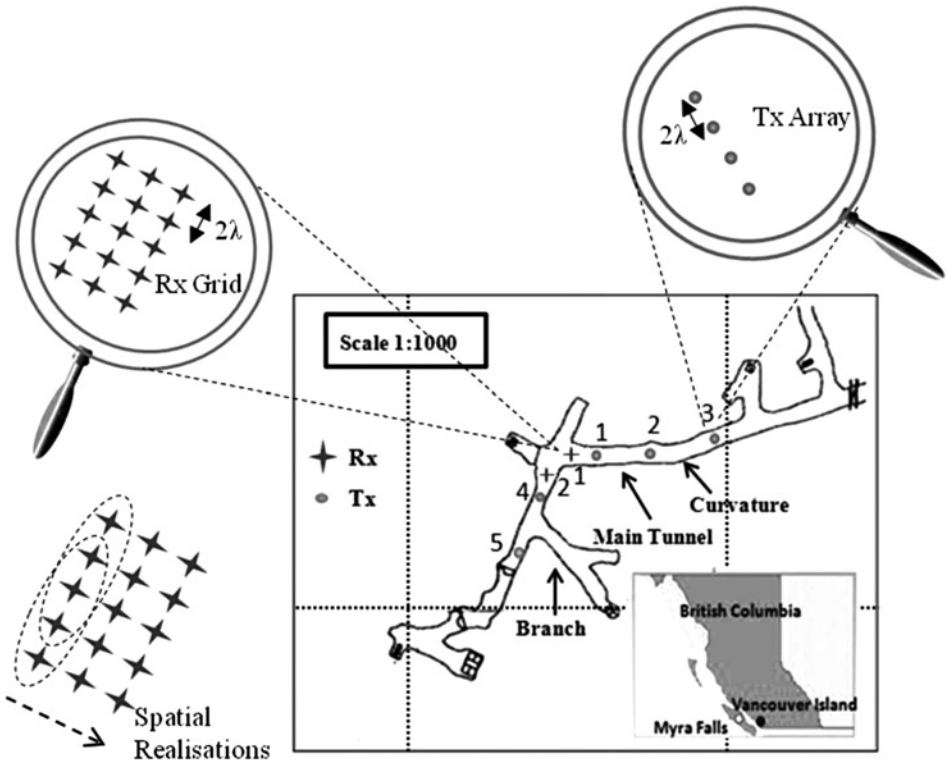

Fig. 1 *Map of the Myra Falls mine in B.C., Canada and the transmitter (Tx) array and receiver (Rx) grid locations (five Tx array locations and two Rx grid locations)*

doi: 10.1049/iet-map.2013.0102

tunnel and was connected to the VNA using an RF-over-fibre range extender. The receiver antenna was automatically moved on a fixed *xy*-positioner (1 × 0.5 m). Locations of the receiver (Rx) grid and transmitter (Tx) array in the mine are demonstrated in Fig. 1. For each transmitter position, the frequency dependent transfer function between the transmitter antenna and all 15 virtual receivers was measured.

2.2 Measurement scenarios

In spite of time constraints in the mine, spatial samples were collected from various parts of the tunnel. Measurement scenarios for different propagation scenarios, such as LOS, NLOS after a curvature etc. are as follows: short-distance LOS (10 m, Tx1–Rx1), long-distance LOS (27 m, Tx2–Rx1), curve-shaped NLOS (49 m, Tx3–Rx1), NLOS in a branch (12 m, Tx4–Rx1) and LOS with a branch in the middle (21 m, Tx5–Rx2). All of these measurements can be considered as typical scenarios in underground mines. As shown in Fig. 1 and Table 1, five sets of measurements were taken: four Tx locations (Tx1–Tx4) for Rx1 and one Tx location (Tx5) for Rx2. At the Tx locations, four antenna positions with a separation of two*wavelengths (2λ) (at 2.49 GHz) were considered in the middle of the tunnel cross section. At the Rx locations, the virtual array was implemented by using a *xy*-positioner with 15 evenly spaced points. Location Rx1 was used for all but one of the scenarios, in which a branch was located in the middle of the direct Tx–Rx path.

2.3 Measurement design: Since no previous work has determined the sufficient spacing required for multiple antenna measurements in underground mines, we investigated previous studies on similar linear confined spaces to select the minimum separation. Several studies in hallways show that the coherence distance is larger than λ [7, 8], and thus the common separation of $\lambda/2$ for conventional indoor environments is not sufficient. In addition to hallways, we considered results of our earlier ray-tracing study and development runs in a mid-size service tunnel (width = 2.7 m, height = 2.4 m and length = 103.5 m). A transmitter and a receiver grid with vertically polarised antennas were located about 35 m apart and in the middle of the tunnel. Since the highest correlations correspond to successive elements, we chose Pearson's correlation coefficient of successive elements (m, n) at the Rx grid for Tx antenna as follows

$$\rho_{hm,hn} = \mathrm{Corr}(h_m,\ h_n) = \frac{E\left[(h_m - \mu_{hm})(h_n - \mu_{hn})\right]}{\sigma_{hm}\sigma_{hn}} \quad (1)$$

where h_m and h_n are channel coefficients corresponding to m and n channels, and also μ and σ represent mean and standard deviations, respectively. The envelope correlation coefficients for two separations of $\lambda/2$ and 2λ were found to be 0.82 and 0.18, respectively. Based on this result and previous work in hallways, we chose 2λ spacing between antenna elements for the Tx array and the Rx grid.

To see the impact of array height, we considered two heights of under the ceiling (2.7 m above ground) and medium height (1.7 m above ground), and to study the impact of antenna polarisation, for both vertical and horizontal antenna polarisations, measurements were performed at medium height. In summary, we collected data for three antenna scenarios: (i) ceiling height with vertically polarised antennas (CV configuration), (ii) medium height for vertically polarised antennas (MV configuration) and (iii) medium height for horizontally polarised antennas (MH configuration). For all the Rx grid points, we performed frequency domain measurement and collected amplitude and phase of the channel gain over the frequency range of 2.49–4 GHz. Measurement scenarios are summarised in Table 1.

To select the suitable array orientation, Pearson's correlation of successive antenna elements was found for two orientations, one perpendicular and one parallel to the tunnel axis. Fig. 2 shows how successive antenna elements are chosen for each array orientation. Results of envelope correlation coefficients for all measurement scenarios are summarised in Table 2. Correlation coefficient values consider all four Tx antennas (i.e. Tx array) for each measurement scenario.

As can be seen in Table 2, array orientation perpendicular to the tunnel axis offers much lower correlation compared with the array orientation parallel to the tunnel axis. Choosing array orientation to be perpendicular to the tunnel axis with its elements separated by 2λ provides a sufficient degree of decorrelation (less than 0.7) regardless of the antenna polarisation, height and propagation scenario. Intuitively, this orientation provides suitable decorrelation

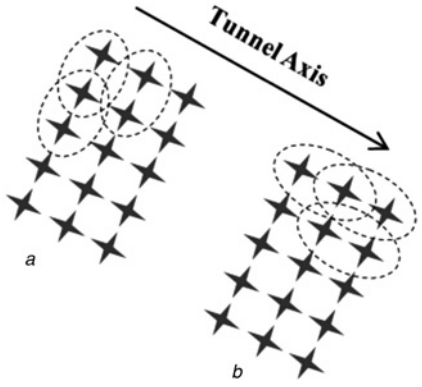

Fig. 2 *Spatial correlation analysis on the successive antenna elements on the Rx grid for two different array orientations*

a Perpendicular to the tunnel axis
b Parallel to the tunnel axis

Table 1 MIMO measurement scenarios in the Myra Falls underground mine

	Tx1 array at Loc. 1	Tx2 array at Loc. 2	Tx3 array at Loc. 3	Tx4 array at Loc. 4	Tx5 array at Loc. 5
Rx1 grid	LOS (10 m) MV	LOS (27 m) (before a curve) MH, MV and CV	NLOS (49 m) (after a curve) MH, MV and CV	NLOS (12 m) (in a branch) MH, MV and CV	—
Rx2 grid	—	—	—	—	LOS (21 m) (a branch in the middle) CV

Table 2 Envelope correlation coefficients of Rx grid antennas for different measurement scenarios (f = 2.49 GHz)

	Rx array orientation perpendicular to the tunnel's axis			Rx array orientation parallel the tunnel's axis		
	MH	MV	CV	MH	MV	CV
Loc. 1 LOS (10 m)	—	0.24	—	—	0.40	—
Loc. 2 LOS (27 m) before curvature	0.21	0.10	0.63	0.67	0.75	0.86
Loc. 3 NLOS (49 m) after curvature	0.30	0.46	0.07	0.83	0.76	0.80
Loc. 4 NLOS (12 m)	0.40	0.07	0.27	0.47	0.54	0.59
Loc. 5 LOS (21 m) branch-middle	–	–	0.45	–	–	0.91

as it occupies the largest space orthogonal to the arriving signals. Therefore we chose this array orientation with element separation of 2λ for constructing 4×4-MIMO $\boldsymbol{H}$-matrices. Although such considerations for array design have not been evaluated for underground mines, the results of capacity analysis will determine whether this design is appropriate or not.

3 Multiple antenna analysis

3.1 Constructing channel coefficient matrices

We started MIMO analysis, after ensuring the absence of large-scale fading across the chosen Tx array. This was examined by averaging the channel power over all the frequencies and Rx grid points on the positioner for each Tx location and comparing them all. Then, as shown in Fig. 1, six 4×4-MIMO spatial realisations based on uniform-linear-arrays (ULAs) oriented perpendicular to the tunnel axis, are constructed (from the fourth-element Tx array and 3×5-element Rx grid). In addition to spatial realisations, 551 frequency samples over range of 2.49–4 GHz and separated by 2.74 MHz were collected. We chose the number of MIMO antenna elements to be four for the following reasons: (i) based on the IEEE-802.11n standard, the maximum allowable MIMO streams is four and (ii) in most environments system performance will significantly increase using two or three antennas, however, by further increase to four the expected capacity improvement may not be achievable (because of increase in correlation among the MIMO subchannels), and therefore worth studying.

For our analysis, we consider a bandwidth of 96 MHz (35 frequency samples). However, because frequency samples within one coherence bandwidth (BW_c) are correlated, all 35 samples cannot be treated as independent. Adding frequency samples to our spatial ones requires them to be independent, which implies separation of at least one BW_c between them [9]. Coherence bandwidth was found to be 4 MHz from the channel-frequency-response. Therefore only half (17 samples) of the 35 frequency samples (with separation of 2.74 MHz) can be considered independent. As a result, 102 (17×6) 4×4-MIMO $\boldsymbol{H}$-matrices were constructed at each location.

3.2 H-matrix normalisation and channel capacity

It is a common practice in MIMO antenna design to normalise $\boldsymbol{H}$-matrices, so that the average SNR at the receiver elements is set to a fixed value and can be adjusted as a parameter. Depending on the objective of MIMO analysis, different methods can be used to calculate the normalisation factor. In order to perform a fair comparison of different systems or schemes, it is required to consider one normalisation factor for all scenarios under the study. Here, two normalisation factors are considered for performance comparison of different antenna scenarios. The choice of normalisation factor depends on whether the objective is to study the effects of: (i) subchannels' correlation only or (ii) both correlation and power, on the capacity.

For normalisation (1), every $\boldsymbol{H}$-matrix is normalised by its own Frobenius norm, which is the RMS value of the elements of a matrix and calculated as follows [10]

$$\boldsymbol{H}_{\text{nor}} = \boldsymbol{H}\sqrt{\frac{N_{\text{Tx}}N_{\text{Rx}}}{\|\boldsymbol{H}\|_F^2}}$$
$$\|\boldsymbol{H}\|_{\mathbf{F}} = \sqrt{\sum_{i=1}^{N_{\text{Rx}}}\sum_{j=1}^{N_{\text{Tx}}}\left|h_{ij}\right|^2} \tag{2}$$

where $\|.\|_{\mathbf{F}}$ denotes Frobenius norm and $\boldsymbol{H}$, N_{Rx}, N_{Tx} and h_{ij} are channel coefficient matrixes, number of Rx antennas, number of Tx antennas and channel matrix entries, respectively. Normalised $\boldsymbol{H}$-matrices obtained by this method are only affected by the level of correlation experienced by the antennas.

Normalisation (2) is often used for fair comparison between different MIMO scenarios (antenna polarisation, array height etc.) or to study the effect of something (e.g. curvature) on the MIMO performance [4, 9]. This normalisation method, which is also called global channel normalisation [11], not only includes subchannels' correlation, but also power contribution of each case. For this normalisation method, a common normalisation factor is considered for all scenarios under comparison, which is calculated based on averaging Frobenius norms of $\boldsymbol{H}$-matrices of all cases being compared. Considering K total channel realisations at each transmitter location, this normalisation can be calculated as follows

$$\boldsymbol{H}_{\text{nor}} = \boldsymbol{H}\sqrt{\frac{KN_{Tx}N_{Rx}}{\|\boldsymbol{H}\|^2}}$$
$$\|\boldsymbol{H}\| = \sqrt{\sum_{k=1}^{K}\sum_{i=1}^{N_{Rx}}\sum_{j=1}^{N_{Tx}}\left|h_{ij}\right|^2} \tag{3}$$

Note that in both methods, the effect of the antenna gain (biconical at 2.49 GHz) and the pathloss between the transmitter and receiver have been excluded. After finding normalised $\boldsymbol{H}$-matrices, capacity C (bit/s/Hz) of a MIMO system with N_{Tx} transmit antennas and N_{Rx} receive antennas can be calculated by Foschini and Gans [10]

$$C = \log_2\left[\det\left(\boldsymbol{I}_{N_{\text{Rx}}} + \frac{\text{SNR}}{N_{\text{Tx}}}\boldsymbol{H}_{\mathbf{nor}}\boldsymbol{H}_{\mathbf{nor}}^{*}\right)\right] \tag{4}$$

where * denotes the transpose-conjugate, $\boldsymbol{H}_{\mathbf{nor}}$ is the $N_{\text{Rx}} \times N_{\text{Tx}}$ normalised channel matrix, SNR is the average signal-to-noise ratio and $\boldsymbol{I}$ is the identity matrix. It is assumed that the N_{Tx} sources have equal power and are uncorrelated.

doi: 10.1049/iet-map.2013.0102

4 Measurement results and discussion

4.1 Performance comparison of MIMO antenna scenarios

Channel capacity, which is the performance measure of MIMO systems, is influenced by two main factors: subchannels' power and the level of spatial correlation among subchannels. Therefore to study the effect of array properties on the MIMO channel capacity, we chose to determine how each array property impacts these two factors. First, we assess them based on their impact on spatial correlation without considering their contribution in power, and afterwards we include the power aspect too. This can be done by applying different normalisation methods to the ***H***-matrices.

4.1.1 Channel capacity without power considerations: In this section, channel capacity CDFs have been found for different measurement scenarios and the pathloss between the centres of the Tx array and Rx grid is calculated, while the antenna element gain and array's power impact (differences because of the array height and antenna polarisation) at each Rx grid are excluded. Therefore the degree of subchannels' decorrelation is the only factor that controls the capacity. This has been done by normalising every ***H***-matrix by its own Frobenius norm [normalisation (1)]. Fig. 3 presents the capacity CDFs of measured channels alongside the CDF of an i.i.d. Rayleigh fading channel to compare the measured channels to an ideal channel, in terms of MIMO performance. As Fig. 3 shows, the capacity CDFs for different antenna heights and polarisations are similar and close to that of an i.i.d. Rayleigh fading channel. This implies that sufficient spacing and properly chosen array orientation provide a sufficient degree of decorrelation regardless of the antenna polarisation and height. However, further analysis is required to see whether they impact subchannels' power. We can also see that the spatial decorrelation achieved by the proposed array is not sensitive to the propagation scenario in the mine.

Another way of analysing the spatial structure of MIMO subchannels is to study singular values of ***H***-matrices. Average singular values corresponding to different measurement scenarios in the mine are presented in Table 3. All singular values are normalised to the largest singular value. Table 3 also confirms that spatial structure of the wireless channel is very close to that of an i.i.d.

Table 3 Singular values of measured ***H***-matrices and i.i.d. Rayleigh ***H***-matrices (all singular values are normalised to the largest one)

		Average singular values			
		σ_1	σ_2	σ_3	σ_4
i.i.d. Rayleigh channel		1	0.69	0.40	0.14
Loc. 1 (10 m)	MV	1	0.71	0.39	0.14
Loc. 2 (27 m)	CV	1	0.55	0.34	0.15
	MH	1	0.67	0.39	0.15
	MV	1	0.63	0.33	0.11
Loc. 3 (49 m)	CV	1	0.70	0.38	0.14
	MH	1	0.67	0.39	0.16
	MV	1	0.55	0.30	0.10
Loc. 4 (12 m)	CV	1	0.67	0.36	0.13
	MH	1	0.69	0.40	0.14
	MV	1	0.70	0.44	0.15
Loc. 5 (21 m)	CV	1	0.61	0.32	0.12

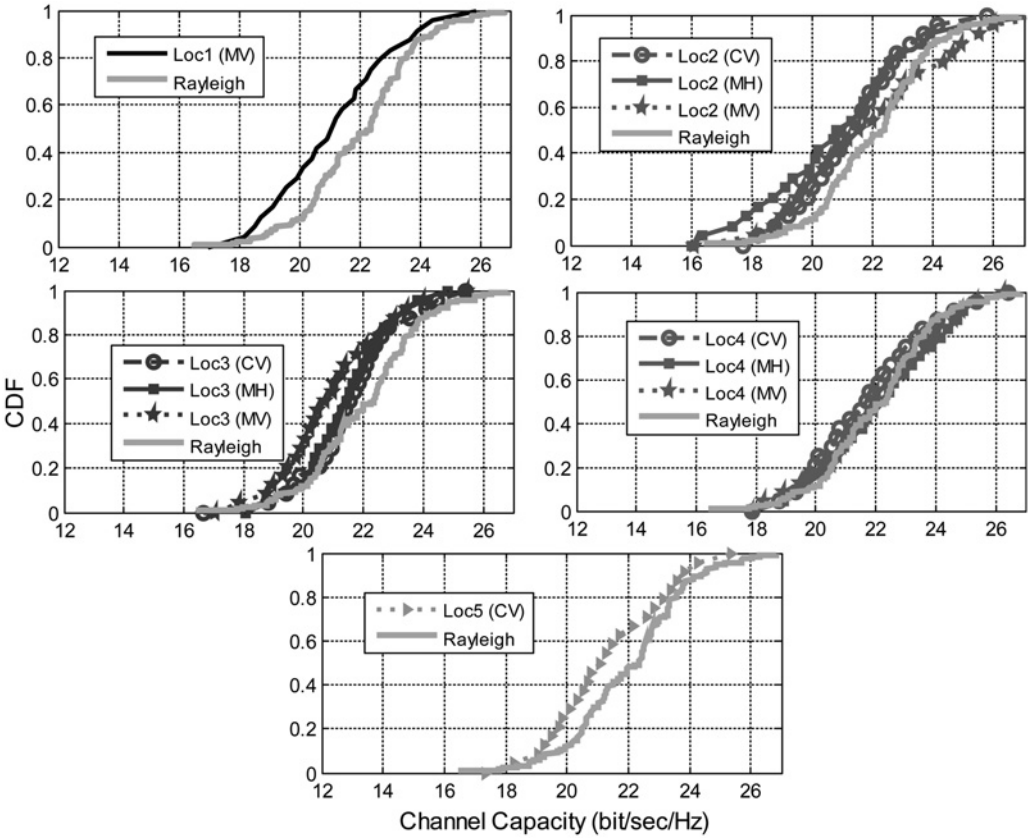

Fig. 3 *CDFs of 4 × 4-MIMO capacity without power considerations (based on the measurement)*

Rayleigh channel (rich-multipath channel), and provides required decorrelation among subchannels. Therefore the spatial structure of the wireless channel is suitable and has the potential for achieving multiplexing gain. The rich-multipath for close Tx–Rx distances has also been reported in other studies [12, 13]. In [13], several amplitude distributions, such as Nakagami, Gamma, Rice, Rayleigh and Lognormal, are tested to model small-scale fading. Using a Kolmogorov–Smirnov's goodness-of-fit test, the authors have shown that the measured LOS scenario (1–12 m) can be modelled by both Nakagami and Rayleigh distributions.

To provide a physical explanation and justification for observing decorrelated MIMO subchannels in the short underground mine tunnel, we have employed the multimode waveguide model, which has been developed and used by Sun and Akyildiz [6] to characterise wireless propagation in underground tunnels. In this model, a tunnel is considered to be an oversized dielectric waveguide and the modes obtained by the waveguide theory are all possible solutions of Maxwell's equations that can exist in the tunnel. We also used this model for MIMO channel characterisation and evaluation of our experimental results in the underground mine tunnel. More details, including the mathematical expressions of this model for tunnels with rectangular cross-sectional shape, can be found in [6].

Angular spread is a key indicator that shows whether a wireless propagation environment has the potential of offering spatially decorrelated subchannels or not. Larger angular spread offers higher spatial decorrelation (or equivalently lower correlation) among the multiple antennas. To characterise the angular spread, we applied the multimode waveguide model to an equivalent rectangular tunnel with the same cross section as size of the Myra Falls mine (width: 5.5 m and height: 4 m). Angular spread in a tunnel can be found as follows [14]

$$\varphi_{\text{rms}} = \sqrt{\frac{\int_{-\pi/2}^{+\pi/2} (\varphi - \bar{\varphi})^2 A(\varphi) \mathrm{d}\varphi}{\int_{-\pi/2}^{+\pi/2} A(\varphi) \mathrm{d}\varphi}}$$
$$\bar{\varphi} = \frac{\int_{-\pi/2}^{+\pi/2} \varphi A(\varphi) \mathrm{d}\varphi}{\int_{-\pi/2}^{+\pi/2} A(\varphi) \mathrm{d}\varphi} \tag{5}$$

where φ_{rms} and $A(\varphi)$ are the azimuth angular spread and power azimuth spectrum, respectively. Fig. 4 shows that the angular spread of the near zone area (including 10 m distance) is quite large. This large angular spread in the near zone is the result of strong reflections from the walls. For further distances (more than about 200 m), angular spread becomes very low (about 4°) because of high attenuation of higher order waveguide modes [6]. To improve spatial decorrelation among subchannels at further distances, antenna separation may need to be increased (more than 2λ).

To exploit the potential of the spatial decorrelation offered by the surrounding environment and achieve the multiplexing gain, inter-element spacing of the antenna array should be chosen properly. Fig. 5*a* shows the capacity as a function of distance, and Fig. 5*b* shows capacity CDFs for different antenna separations obtained by using the multimode waveguide model. As can be seen from both figures, the common antenna spacing of the off-the-shelf products ($\lambda/2$) is not sufficient, and does not offer consistent performance

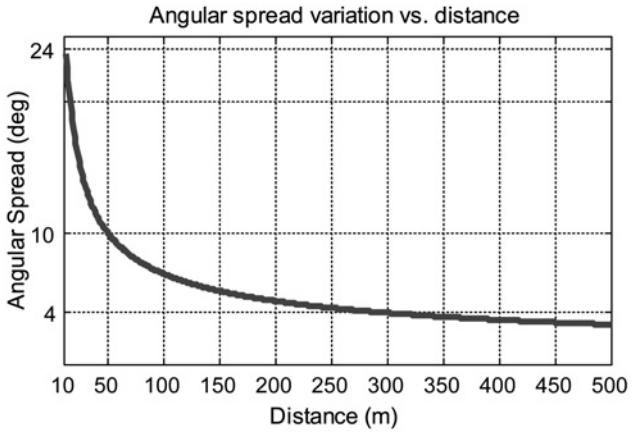

Fig. 4 *Angular spread variation against distance (based on multimode waveguide model)*

over Tx–Rx distance. On the other hand, 2λ separation shows suitable and consistent performance (capacity) and spacing the antennas further than that (e.g. 6λ) does not achieve higher capacity. This confirms our measurement results. For very large Tx–Rx distances however, the element spacing may require to be increased. The capacity CDF for 2λ spacing also matches well with the capacity results measured in the mine.

4.1.2 Channel capacity with power considerations:

To include the power impact of array height and antenna polarisation, Tx–Rx pathloss and antenna element gain have been removed from the ***H***-matrices by considering a common normalisation factor, normalisation (2), for all configurations at each Rx grid. In this way, capacity is calculated so that it includes the impact of antenna

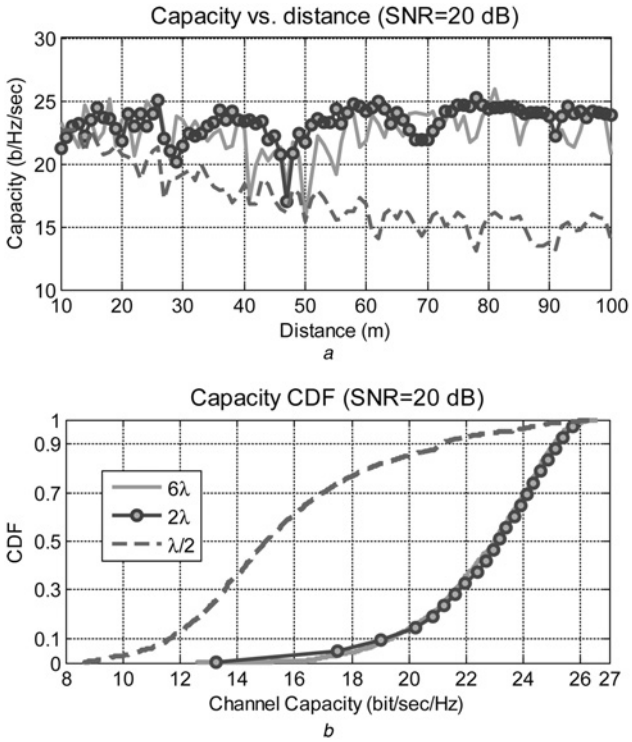

Fig. 5 *Capacity of 4 × 4-MIMO system for different antenna spacings (based on the multimode waveguide model)*

doi: 10.1049/iet-map.2013.0102

polarisation and array height on both subchannels' decorrelation and power. Fig. 6 shows capacity CDFs for different antenna scenarios at different measurement locations. At Loc. 1 and Loc. 5, one antenna configuration was considered, whereas for the rest of the locations three configurations were measured. Comparing all figures, the largest difference among CDFs of antenna configurations is about 5 bit/sec/Hz in after the curvature scenario and between MH/CV with MV configuration.

4.2 Impact of antenna polarisation

Fig. 6 shows similar performance for MH and MV scenarios; however, the MH scenario has a slightly better capacity CDF (about 1 bit/s/Hz) for both Loc. 2 (LOS) and Loc. 4 (NLOS). This similar performance of two polarisations is likely because of the high depolarisation in the near zone of the tunnel. However, because the aspect ratio of the tunnel is horizontal (i.e. tunnel width is larger than tunnel height), horizontal polarisation shows a bit lower attenuation in the near zone. Based on our results, this is only valid for the straight part of the tunnel. In Loc. 3, where a curvature exists between the transmitter and receiver, MV shows the best performance by a large margin (5 bit/s/Hz) for both MH and CV cases. Poor performance of MH in this case, can be attributed to the fact that horizontally polarised waves are attenuated more than vertical ones by the curvature, and thus the degradation of capacity can be because of the power loss.

Similar behaviour has been reported for horizontally polarised waves propagating in a subway tunnel, which is substantially larger than a typical underground mine [15]. Assume a rectangular tunnel as shown in Fig. 7. Equations (6) and (7) give the attenuation of $\boldsymbol{EH}_{mn}$ mode (α_{mn}) in this tunnel for y-polarisation (vertical polarisation) and

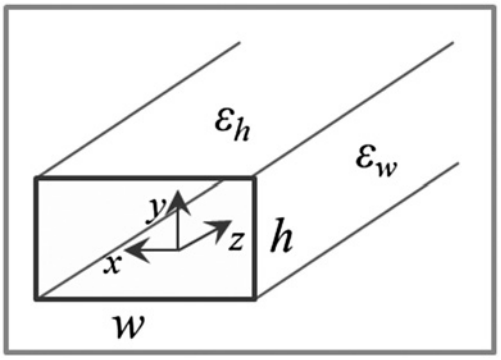

Fig. 7 *Tunnel with rectangular cross section*

x-polarisation (horizontal polarisation), respectively, [15, 16]

$$\alpha_{mn}^{y} = \frac{2}{w}\left(\frac{m\lambda}{2w}\right)^2 \mathrm{Re}\left[\frac{1}{\sqrt{\varepsilon_w - 1}}\right] + \frac{2}{h}\left(\frac{n\lambda}{2h}\right)^2 \mathrm{Re}\left[\frac{\varepsilon_h}{\sqrt{\varepsilon_h - 1}}\right] \quad (6)$$

$$\alpha_{mn}^{x} = \frac{2}{w}\left(\frac{m\lambda}{2w}\right)^2 \mathrm{Re}\left[\frac{\varepsilon_w}{\sqrt{\varepsilon_w - 1}}\right] + \frac{2}{h}\left(\frac{n\lambda}{2h}\right)^2 \mathrm{Re}\left[\frac{1}{\sqrt{\varepsilon_h - 1}}\right] \quad (7)$$

where w, h, λ, ε_w and ε_h are tunnel width, tunnel height, wavelength, relative permittivity of vertical walls (sidewalls) and relative permittivity of horizontal walls (ceiling/floor),

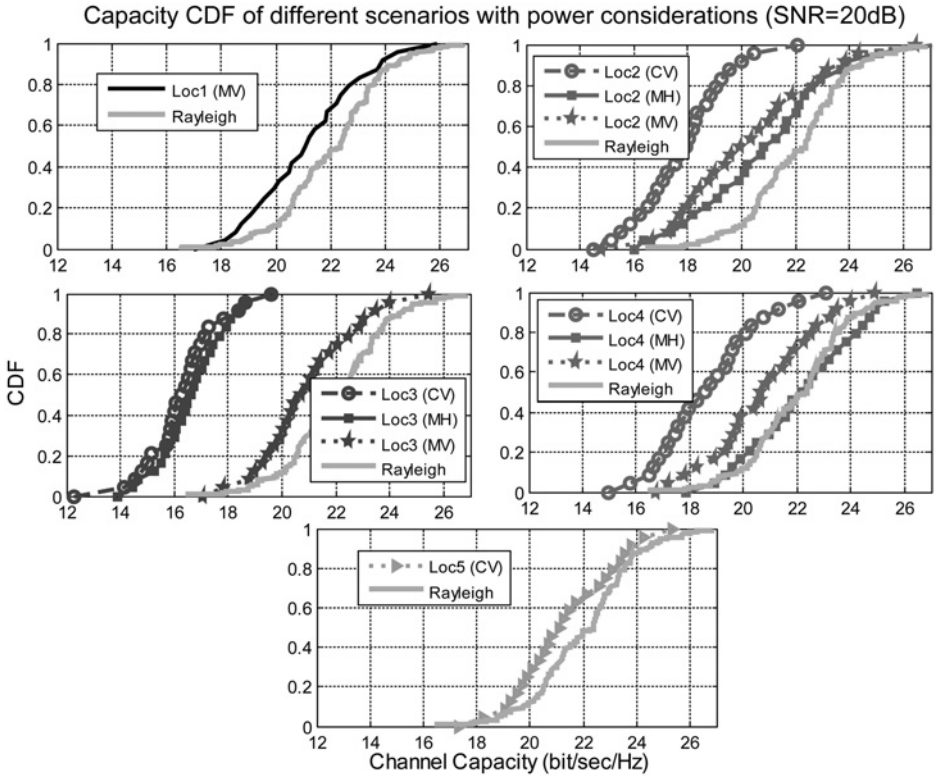

Fig. 6 *CDFs of 4 × 4-MIMO capacity with power considerations (based on the measurement)*

Table 4 Mean pathloss measured at each Rx grid location in Myra Falls mine (at 2.49 GHz)

		Mean pathloss, dB (including the antenna gain)			Free space pathloss, dB
Loc. 1 LOS (10 m) MV	Tx1_antenna1		−62.31		−60.36
	Tx1_antenna2		−60.42		
	Tx1_antenna3		−59.64		
	Tx1_antenna4		−60.52		
		CV	MV	MH	
Loc. 2 LOS (27 m)before curvature CV, MH and MV	Tx2_antenna1	−69.84	−68.19	−67.71	−69.00
	Tx2_antenna2	−69.71	−68.46	−68.54	
	Tx2_antenna3	−71.43	−69.89	−68.85	
	Tx2_antenna4	−71.24	−70.51	−68.73	
Loc. 3NLOS (49 m) after curvature CV, H and MV	Tx3_antenna1	−83.19	−78.62	−83.56	−74.17
	Tx3_antenna2	−81.66	−79.67	−82.04	
	Tx3_antenna3	−82.14	−77.59	−81.02	
	Tx3_antenna4	−83.08	−76.93	−82.00	
Loc.4 NLOS (12 m) CV, MH and MV	Tx4_antenna1	−80.30	−78.18	−77.79	−62.00
	Tx4_antenna2	−80.54	−78.63	−76.75	
	Tx4_antenna3	−80.05	−78.34	−77.64	
	Tx4_antenna4	−80.22	−79.57	−78.44	
Loc. 5 LOS (21 m) branch-middle CV	Tx5_antenna1	−72.65			−66.82
	Tx5_antenna2	−70.97			
	Tx5_antenna3	−71.55			
	Tx5_antenna4	−68.08			

respectively. As can be seen from (7), vertical walls (sidewalls) on which horizontally polarised $\boldsymbol{E}$ is perpendicular to, contribute to most of the attenuation [16]. In [16], it is shown that if $\boldsymbol{E}$ is perpendicular to the curved walls, more attenuation occurs because of additional loss caused by the curvature. In fact, curvature of the sidewalls can be considered as a polarisation filter that passes only vertically polarised waves, and its level of filtering is inversely proportional to the radius of the curvature.

4.3 Impact of array height

For all the Rx locations with CV scenario, we can see that the ceiling height shows lower capacity compared with the middle height. Capacity median is found to be 2–5 bit/s/Hz less at the ceiling height compared with the middle one (MV). Based on the waveguide theory, antenna located in the middle of the tunnel can couple higher power to the tunnel because of excitation and reception of the dominant propagation mode. Although it may not be practical to place the antenna array in the middle of the tunnel, this result suggests placing the antenna further from the ceiling for short underground tunnels. If this is not possible because of practical considerations, reduction on capacity should be taken into account while designing MIMO systems. This result may not necessarily be valid for very long Tx–Rx distances. Over very long distances (several 100 m or more), only a limited number of waveguide propagation modes exist because the higher order modes are significantly attenuated. Higher order modes, acting like multipath components are an important factor to construct spatially decorrelated MIMO subchannels. Therefore to excite higher order modes with sufficient energy to remain active for long distances, off-centred position of Tx and Rx arrays in the transverse plane may be preferred over centred position, as described in [4]. This implies that at far distances a trade-off may be required between subchannels' power and decorrelation.

To evaluate results obtained in this section, Table 4 compares the mean pathloss between each Tx antenna and Rx grid for each measurement scenario. Free space pathloss which is calculated considering a longitudinal distance between the centre of the transmitter array and centre of the Rx grid, is also given. As it can be seen, MH shows the lowest pathloss at Loc. 2 and Loc. 4, while showing the highest one at Loc. 3 (after the curvature). We can also see relatively similar performance for both polarisations at Loc. 2 and Loc. 4, and better performance for the middle height compared with the ceiling height. These results match results obtained from Fig. 5, and thus confirm previous discussion on different power contributions of different array configurations.

Experimental results of capacity predictions with power considerations are compared with results from the multimode waveguide model for two LOS cases between 10 and 27 m in the straight part of the mine. Figs. 8*a–d* compare capacity CDFs obtained by measurement and multimode model for Loc. 1 and Loc. 2, respectively. In Fig. 8*b–d*, capacity CDFs from the multimode waveguide model for different heights and polarisations are obtained based on normalisation (2). The experimental results match well with the theoretical results obtained for both locations, heights and polarisations. This indicates that the multimode waveguide model can be considered as a simulation tool to effectively design and deploy advanced systems, such as MIMO-based devices in mine tunnels.

5 Conclusions

By this study, we showed that antenna array properties such as array orientation, height, antenna spacing and polarisation greatly impact the performance of MIMO systems in underground mines. Our experimental and theoretical analyses revealed that deploying fourth-element ULAs with element separation of 2λ, horizontal orientation and placed perpendicular to the tunnel axis provides a sufficient degree of decorrelation among subchannels to achieve a suitable MIMO capacity (close to that of an i.i.d. Rayleigh fading channel) in several propagation scenarios studied in a short underground mine tunnel.

doi: 10.1049/iet-map.2013.0102

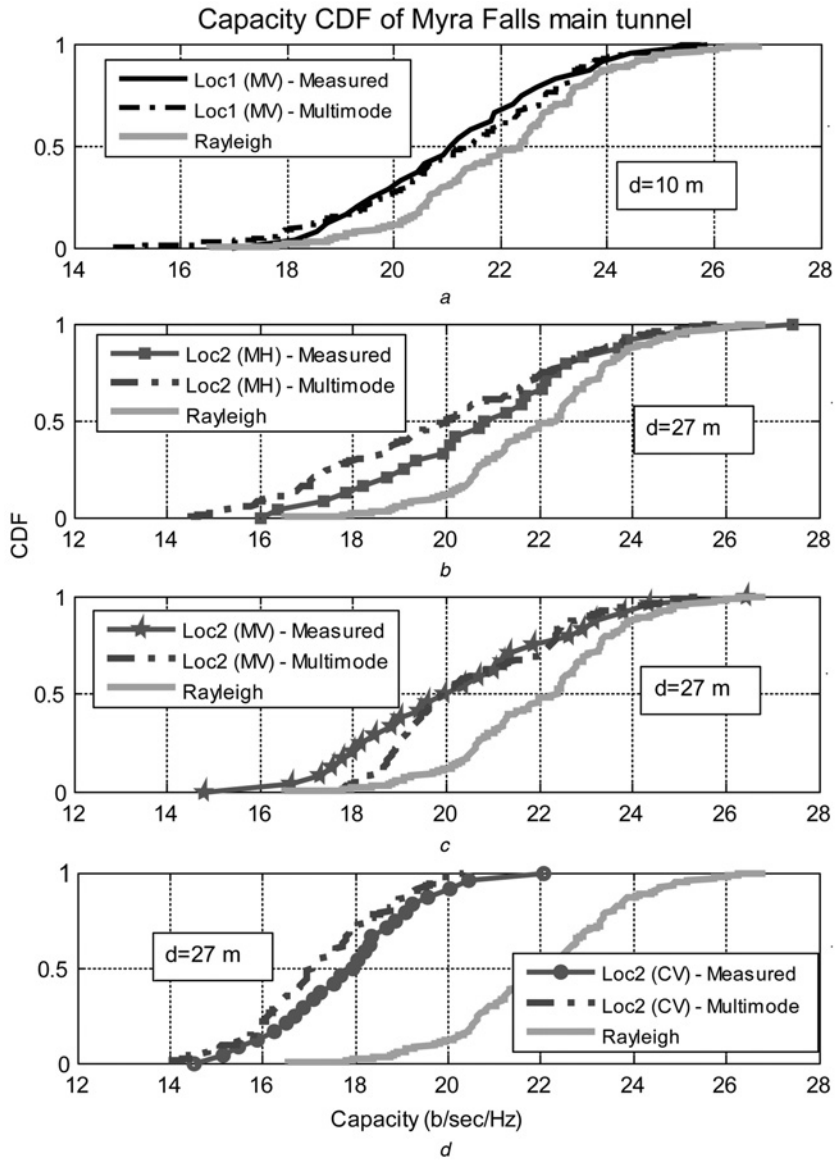

Fig. 8 *CDFs of 4 × 4-MIMO capacity with power considerations (based on measurement and multimode waveguide model at f = 2.49 GHz and SNR = 20 dB)*

We showed that if MIMO antenna arrays are deployed based on the proposed array orientation and inter-element separation, array height and antenna polarisation will mainly impact the power of MIMO subchannels without significantly changing their spatial structure. This implies that by employing the proposed array design, one can choose other antenna properties (e.g. antenna polarisation and height) while devoting main focus on power aspects (similar to SISO systems) rather than concerning about the spatial correlation among MIMO subchannels.

We also confirmed previous studies by showing that the mine geometry is a key factor that should be taken into account while designing wireless systems for underground tunnels. As an example, although in mines with a horizontal aspect ratio, horizontally polarised antennas show lower attenuation, and thus are more desirable, if a curvature exists between the transmitter and receiver, vertical polarisation is preferred as it is much less affected by the curvature loss.

In spite of the dissimilarities between underground mines and tunnels, some of our results confirm and support results obtained in subway tunnels. Nevertheless, because underground mines are geometrically diverse, more measurement campaigns in various mines are required to reconfirm previous findings and reveal new physical trends or principles.

6 Acknowledgments

The authors thank the Natural Sciences and Engineering Research Council (NSERC) of Canada and the British Columbia Innovation Council (BCIC) for supporting this research. The authors also thank Nystar Mining for providing them with access to their Cu-Pb–Zn mine near Myra Falls on Vancouver Island for the purpose of collecting measurement data.

7 References

1 Lienard, M., Degauque, P., Baudet, J., Degardin, D.: 'Investigation on MIMO channels in subway tunnels', *IEEE J. Sel. Areas Commun.*, 2003, **21**, (3), pp. 332–339

2 Molina-Garcia-Pardo, J., Lienard, M., Stefanut, P., Degauque, P.: 'Propagation in tunnels: experimental investigations and channel modeling in a wide frequency band for MIMO applications', *EURASIP J. Wirel. Commun. Netw.*, 2009, **2006**, pp. 1–9

3 Lienard, M., Degauque, P.: 'MIMO communication in tunnels: influence of the range and of the tunnel geometry on system performances'. Proc. Wireless Communications Systems Villeneuve d'Ascq, France, September 2004, pp. 290–293

4 Molina-Garcia-Pardo, J., Lienard, M., Degauque, P., Dudley, D.G., Juan-Llacer, L.: 'Interpretation of MIMO channel characteristics in rectangular tunnels from modal theory', *IEEE Trans. Veh. Technol.*, 2008, **57**, (3), pp. 1974–1979

5 Ben Mabrouk, I., Talbi, L., Nedil, M.: 'Performance evaluation of a MIMO system in underground mine gallery', *IEEE Antennas Propag. Lett.*, 2012, **11**, pp. 830–833

6 Sun, Z., Akyildiz, I.F.: 'Channel modeling and analysis for wireless networks in underground mines and road tunnels', *IEEE Trans. Commun.*, 2010, **58**, (6), pp. 1758–1768

7 Svantesson, T., Wallace, J.: 'Statistical characterization of the indoor MIMO channel based on LOS/NLOS measurements'. Proc. IEEE Signals Systems Computers, Provo, UT, USA, November 2002, pp. 1354–1358

8 Kyritsi, P., Cox, D.C., Valenzuela, R.A., Wolniansky, P.W.: 'Correlation analysis based on MIMO channel measurements in an indoor environment', *IEEE J. Sel. Areas Commun.*, 2003, **21**, (5), pp. 713–720

9 Anreddy, V.R., Ingram, M.A.: 'Capacity of measured Ricean and Rayleigh indoor MIMO channels at 2.4 GHz with polarization and spatial diversity'. Proc. IEEE WCNC'06, 3–6 April 2006, pp. 946–951

10 Foschini, J., Gans, M.: 'On the limit of wireless communications in a fading environment when using multiple antennas', *Wirel. Pers. Commun.*, 1998, **6**, (3), pp. 311–335

11 Tsoulos, G., MIMO system technology for wireless communications (Electrical Engineering and Applied Signal Processing) (CRC Press, Inc., 2006), p. 194

12 Chehri, A., Fortier, P., Aniss, H., Tardif, P.M., 'UWB spatial fading and small scale characterization in underground mines'. IEEE Communications Biennial Symp., 2006, pp. 213–218

13 Chehri, A., Fortier, P., Tardif, P.M.: 'Characterization of the ultra-wideband channel in confined environments with diffracting rough surfaces', *Wirel. Pers. Commun.*, 2012, **62**, (4), pp. 859–877

14 Garcia-Pardo, C., Molina-Garcia-Pardo, J., Lienard, M., Gaillot, D.P., Degauque, P.: 'Double directional channel measurements in an arched tunnel and interpretation using ray tracing in a rectangular tunnel', *PIERM*, 2012, **22**, pp. 91–107

15 Dudley, D.G., Lienard, M., Mahmoud, S.F., Degauque, P.: 'Wireless propagation in tunnels', *IEEE Antennas Propag. Mag.*, 2007, **49**, (2), pp. 11–26

16 Mahmoud, S.F.: 'Modal propagation of high frequency electromagnetic waves in straight and curved tunnels within the earth', *J. Electromagn. Waves Appl.*, 2005, **19**, (12), pp. 1611–1627

doi: 10.1049/iet-map.2013.0102